High passive CEP stability from a few-cycle, tunable NOPA-DFG system for observation of CEP-effects in photoemission

Jan Vogelsang,[1,2,5] Jörg Robin,[1,2,5] Björn Piglosiewicz,[1,2] Cristian Manzoni,[3] Paolo Farinello,[3] Stefan Melzer,[4] Philippe Feru,[4] Giulio Cerullo,[3] Christoph Lienau,[1,2] and Petra Groß[1,2,*]

[1]*Institut für Physik, Carl von Ossietzky Universität, 26129 Oldenburg, Germany*
[2]*Center of Interface Science, Carl von Ossietzky Universität, 26129 Oldenburg, Germany*
[3]*IFN-CNR, Dipartimento di Fisica, Politecnico di Milano, 20133 Milano, Italy*
[4]*Spectra-Physics, Santa Clara, CA 95054, USA*
[5]*Both authors contributed equally*
**petra.gross@uni-oldenburg.de*

Abstract: The investigation of fundamental mechanisms taking place on a femtosecond time scale is enabled by ultrafast pulsed laser sources. Here, the control of pulse duration, center wavelength, and especially the carrier-envelope phase has been shown to be of essential importance for coherent control of high harmonic generation and attosecond physics and, more recently, also for electron photoemission from metallic nanostructures. In this paper we demonstrate the realization of a source of 2-cycle laser pulses tunable between 1.2 and 2.1 μm, and with intrinsic CEP stability. The latter is guaranteed by difference frequency generation between the output pulse trains of two noncollinear optical parametric amplifier stages that share the same CEP variations. The CEP stability is better than 50 mrad over 20 minutes, when averaging over 100 pulses. We demonstrate the good CEP stability by measuring kinetic energy spectra of photoemitted electrons from a single metal nanostructure and by observing a clear variation of the electron yield with the CEP.

OCIS codes: (320.7120) Ultrafast phenomena; (190.4410) Nonlinear optics, parametric processes; (320.7110) Ultrafast nonlinear optics; (270.6620) Strong-field processes.

References and links

1. E. Goulielmakis, Z.-H. Loh, A. Wirth, R. Santra, N. Rohringer, V. S. Yakovlev, S. Zherebtsov, T. Pfeifer, A. M. Azzeer, M. F. Kling, S. R. Leone, and F. Krausz, "Real-time observation of valence electron motion," Nature **466**(7307), 739–743 (2010).
2. A. Mokhtari, P. Cong, J. L. Herek, and A. H. Zewail, "Direct femtosecond mapping of trajectories in a chemical reaction," Nature **348**(6298), 225–227 (1990).
3. R. R. Alfano and S. L. Shapiro, "Emisson in region 400 to 7000 A via 4-photon oupling in glass," Phys. Rev. Lett. **24**(11), 584–587 (1970).
4. M. Bradler, P. Baum, and E. Riedle, "Femtosecond continuum generation in bulk laser host materials with sub-μJ pump pulses," Appl. Phys. B **97**(3), 561–574 (2009).
5. J. C. Knight, "Photonic crystal fibres," Nature **424**(6950), 847–851 (2003).
6. P. Russell, "Photonic crystal fibers," Science **299**(5605), 358–362 (2003).
7. D. Brida, C. Manzoni, G. Cirmi, M. Marangoni, S. Bonora, P. Villoresi, S. De Silvestri, and G. Cerullo, "Few-optical-cycle pulses tunable from the visible to the mid-infrared by optical parametric amplifiers," J. Opt. **12**(1), 013001 (2010).
8. F. Krausz and M. Ivanov, "Attosecond physics," Rev. Mod. Phys. **81**(1), 163–234 (2009).
9. C. A. Haworth, L. E. Chipperfield, J. S. Robinson, P. L. Knight, J. P. Marangos, and J. W. G. Tisch, "Half-cycle cutoffs in harmonic spectra and robust carrier-envelope phase retrieval," Nat. Phys. **3**(1), 52–57 (2007).
10. J. Itatani, J. Levesque, D. Zeidler, H. Niikura, H. Pépin, J. C. Kieffer, P. B. Corkum, and D. M. Villeneuve, "Tomographic imaging of molecular orbitals," Nature **432**(7019), 867–871 (2004).

#220700 - $15.00 USD Received 8 Aug 2014; revised 26 Sep 2014; accepted 26 Sep 2014; published 9 Oct 2014

11. M. Nisoli, G. Sansone, S. Stagira, S. De Silvestri, C. Vozzi, M. Pascolini, L. Poletto, P. Villoresi, and G. Tondello, "Effects of carrier-envelope phase differences of few-optical-cycle light pulses in single-shot high-order-harmonic spectra," Phys. Rev. Lett. **91**(21), 213905 (2003).
12. M. Krüger, M. Schenk, and P. Hommelhoff, "Attosecond control of electrons emitted from a nanoscale metal tip," Nature **475**(7354), 78–81 (2011).
13. B. Piglosiewicz, S. Schmidt, D. J. Park, J. Vogelsang, P. Gross, C. Manzoni, P. Farinello, G. Cerullo, and C. Lienau, "Carrier-envelope phase effects on the strong-field photoemission of electrons from metallic nanostructures," Nat. Photonics **8**, 38–43 (2014).
14. P. Hommelhoff, C. Kealhofer, and M. A. Kasevich, "Ultrafast Electron Pulses from a Tungsten Tip Triggered by Low-Power Femtosecond Laser Pulses," Phys. Rev. Lett. **97**(24), 247402 (2006).
15. D. J. Park, B. Piglosiewicz, S. Schmidt, H. Kollmann, M. Mascheck, and C. Lienau, "Strong field acceleration and steering of ultrafast electron pulses from a sharp metallic nanotip," Phys. Rev. Lett. **109**(24), 244803 (2012).
16. T. Wilhelm, J. Piel, and E. Riedle, "Sub-20-fs pulses tunable across the visible from a blue-pumped single-pass noncollinear parametric converter," Opt. Lett. **22**(19), 1494–1496 (1997).
17. G. Cerullo and S. De Silvestri, "Ultrafast optical parametric amplifiers," Rev. Sci. Instrum. **74**(1), 1–18 (2003).
18. F. J. Furch, S. Birkner, F. Kelkensberg, A. Giree, A. Anderson, C. P. Schulz, and M. J. J. Vrakking, "Carrier-envelope phase stable few-cycle pulses at 400 kHz for electron-ion coincidence experiments," Opt. Express **21**(19), 22671–22682 (2013).
19. N. Ishii, K. Kitano, T. Kanai, S. Watanabe, and J. Itatani, "Carrier-Envelope-Phase-Preserving, Octave-Spanning Optical Parametric Amplification in the Infrared Based on BiB3O6 Pumped by 800nm Femtosecond Laser Pulses," Appl. Phys. Express **4**(2), 022701 (2011).
20. S. T. Cundiff, "Phase stabilization of ultrashort optical pulses," J. Phys. D Appl. Phys. **35**(8), R43–R59 (2002).
21. T. Fuji, J. Rauschenberger, A. Apolonski, V. S. Yakovlev, G. Tempea, T. Udem, C. Gohle, T. W. Hänsch, W. Lehnert, M. Scherer, and F. Krausz, "Monolithic carrier-envelope phase-stabilization scheme," Opt. Lett. **30**(3), 332–334 (2005).
22. O. D. Mücke, R. Ell, A. Winter, J. W. Kim, J. R. Birge, L. Matos, and F. X. Kärtner, "Self-referenced 200 MHz octave-spanning Ti: sapphire laser with 50 attosecond carrier-envelope phase jitter," Opt. Express **13**(13), 5163–5169 (2005).
23. S. Rausch, T. Binhammer, A. Harth, E. Schulz, M. Siegel, and U. Morgner, "Few-cycle oscillator pulse train with constant carrier-envelope- phase and 65 as jitter," Opt. Express **17**(22), 20282–20290 (2009).
24. G. Cerullo, A. Baltuška, O. D. Mücke, and C. Vozzi, "Few-optical-cycle light pulses with passive carrier-envelope phase stabilization," Laser Photonics Rev. **5**(3), 323–351 (2011).
25. A. Baltuska, T. Fuji, and T. Kobayashi, "Controlling the carrier-envelope phase of ultrashort light pulses with optical parametric amplifiers," Phys. Rev. Lett. **88**(13), 133901 (2002).
26. G. Krauss, D. Fehrenbacher, D. Brida, C. Riek, A. Sell, R. Huber, and A. Leitenstorfer, "All-passive phase locking of a compact Er:fiber laser system," Opt. Lett. **36**(4), 540–542 (2011).
27. C. Manzoni, G. Cerullo, and S. De Silvestri, "Ultrabroadband self-phase-stabilized pulses by difference-frequency generation," Opt. Lett. **29**(22), 2668–2670 (2004).
28. C. Vozzi, G. Cirmi, C. Manzoni, E. Benedetti, F. Calegari, G. Sansone, S. Stagira, O. Svelto, S. De Silvestri, M. Nisoli, and G. Cerullo, "High-energy, few-optical-cycle pulses at 1.5 μm with passive carrier-envelope phase stabilization," Opt. Express **14**(21), 10109–10116 (2006).
29. C. Homann, M. Bradler, M. Förster, P. Hommelhoff, and E. Riedle, "Carrier-envelope phase stable sub-two-cycle pulses tunable around 1.8 μm at 100 kHz," Opt. Lett. **37**(10), 1673–1675 (2012).
30. M. Bradler, C. Homann, and E. Riedle, "Broadband difference frequency mixing between visible and near-infrared pulses for few-cycle pulse generation with stable carrier-envelope phase," Appl. Phys. B **113**(1), 19–25 (2013).
31. G. Cerullo, M. Nisoli, S. Stagira, and S. De Silvestri, "Sub-8-fs pulses from an ultrabroadband optical parametric amplifier in the visible," Opt. Lett. **23**(16), 1283–1285 (1998).
32. I. Amat-Roldán, I. Cormack, P. Loza-Alvarez, E. Gualda, and D. Artigas, "Ultrashort pulse characterisation with SHG collinear-FROG," Opt. Express **12**(6), 1169–1178 (2004).
33. M. Kakehata, H. Takada, Y. Kobayashi, K. Torizuka, Y. Fujihira, T. Homma, and H. Takahashi, "Single-shot measurement of carrier-envelope phase changes by spectral interferometry," Opt. Lett. **26**(18), 1436–1438 (2001).
34. C. Feng, J. F. Hergott, P. M. Paul, X. Chen, O. Tcherbakoff, M. Comte, O. Gobert, M. Reduzzi, F. Calegari, C. Manzoni, M. Nisoli, and G. Sansone, "Complete analog control of the carrier-envelope-phase of a high-power laser amplifier," Opt. Express **21**(21), 25248–25256 (2013).
35. T. Wittmann, B. Horvath, W. Helml, M. G. Schaetzel, X. Gu, A. L. Cavalieri, G. G. Paulus, and R. Kienberger, "Single-shot carrier-envelope phase measurement of few-cycle laser pulses," Nat. Phys. **5**(5), 357–362 (2009).
36. B. Borchers, A. Anderson, and G. Steinmeyer, "On the role of shot noise in carrier- envelope phase stabilization," Laser Photonics Rev. **8**(2), 303–315 (2014).
37. A. Guandalini, P. Eckle, M. Anscombe, P. Schlup, J. Biegert, and U. Keller, "5.1 fs pulses generated by filamentation and carrier envelope phase stability analysis," J. Phys. At. Mol. Opt. Phys. **39**(13), S257–S264 (2006).

#220700 - $15.00 USD Received 8 Aug 2014; revised 26 Sep 2014; accepted 26 Sep 2014; published 9 Oct 2014

38. B. Piglosiewicz, J. Vogelsang, S. Schmidt, D. J. Park, P. Gross, and C. Lienau, "Electron Photoemission and Acceleration from Sharp Gold Nanotapers in the Strong-Field, Few-Cycle Regime," Quantum Matter **3**(4), 10 (2014).

1. Introduction

Ultrafast pulsed laser sources are an important tool to directly observe fundamental processes taking place on a femtosecond time scale, such as for example the motion of electron wave packets during electronic excitation of atoms or molecules [1] or during chemical processes [2]. In recent years, the focus for generating such ultrafast laser pulses has shifted from solid-state or fiber-based laser oscillators to white-light (WL) generation in bulk material [3, 4] or nonlinear fibers [5, 6] followed by parametric nonlinear optical processes. Such schemes have been shown to enable generation of few-cycle laser pulses over a wide spectral range from the visible to the far-infrared [7]. Wavelength tunability is important because it allows addressing or avoiding certain material resonances and, more specifically, to minimize local heating of metallic nanostructures by tuning the laser to the red of the onset of interband absorption of the metal. Also, wavelength tuning enables a variation of the quiver oscillation period and hence provides important control over strong field photoemission processes. Wavelenght-flexible light sources thus open the path to investigating different fundamental mechanisms from electronic excitation via vibrational motion to off-resonance strong-field effects, such as high harmonic generation (HHG), attosecond streaking or strong-field tunneling ionization [8].

In the strong-field regime, the electric field strength rather than the peak or average intensity plays a key role. Thus, for very short pulses, the phase of the carrier wave with respect to the pulse envelope, also known as carrier-envelope phase (CEP), determines the maximum strength of the electric field and has been demonstrated to be of key importance for coherent control of HHG and attosecond streaking in gases [9–11]. More recently, similar effects have been demonstrated for photoemission from metallic nanostructures: In the case of multiphoton ionization, CEP effects are ascribed to changing interferences of electron wave packets, which are emitted in subsequent cycles of the driving laser field [12], while in the case of strong-field electron emission the changing maximum field strength directly influences the electron motion [13]. The latter indicates control of electron motion via the laser field and may become an enabling step towards the generation and application of attosecond electron pulses.

Experiments as the ones described above require ultrafast laser pulses with a duration of only a few cycles, a wavelength in the near-infrared range, and with a stable CEP. Furthermore, the electric field strength must be on the order of the inner-atomic field strength to enable tunneling of the electrons through the potential barrier, however, this condition can be mitigated by exploiting the field enhancement around metallic nanostructures [14, 15]. Noncollinear optical parametric amplifiers (NOPAs) are used since more than a decade. Since then, they have been continuously improved to supply high gain over very wide bandwidths within the whole transparency range of the used nonlinear crystals [16, 17]. It has been shown that NOPAs have the capability of preserving the phase of the amplified light [18, 19], which can be used, e.g., to transfer the phase of an actively CEP-stabilized oscillator [20–23]. Recently, their ability of providing intrinsic, passive CEP stability has moved into focus [24, 25]. Such passive, all-optical schemes can be realized in different setups, but they usually rely on difference frequency generation (DFG) of two pulses with the same CEP [19, 26–30].

Here we present the realization and characterization of a source of few-cycle, passively CEP-stabilized laser pulses tunable between 1.2 and 2.1 μm for controlling photoemission and motion of electrons by the phase of a strong light field. The approach is based on DFG between the output of two NOPAs, which are seeded by the same WL and thus share the same CEP (similar to [27]). We achieve a CEP stability better than 50 mrad over time spans of seconds up to 20 minutes, when averaging over 100 pulses, which is an excellent long-term

#220700 - $15.00 USD Received 8 Aug 2014; revised 26 Sep 2014; accepted 26 Sep 2014; published 9 Oct 2014

CEP stability. The suitability of the CEP-stable laser source for strong-field experiments is demonstrated by measuring kinetic energy spectra of photoemitted electrons from a metallic nano-taper as a function of the CEP.

2. Experimental setup

The experimental setup of the ultrafast pulse source is shown schematically in Fig. 1. Coarsely, our system can be grouped into two parallel NOPA stages followed by DFG, and it is pumped by a chirped pulse regenerative amplifier system (Spectra-Physics Spitfire Pro XP) emitting pulses of 120-fs duration at 800-nm center wavelength with a repetition rate of up to 5 kHz and a pulse energy of 800 μJ. Our approach is to generate pulses with a broad bandwidth (and short duration) at a center wavelength around 600 nm in one stage (NOPA#1), and pulses with a narrow bandwidth at 890 nm in the other stage (NOPA#2). With this choice of wavelength for NOPA#2 the spectral properties of NOPA#1 are transferred to the wavelength region around 1.6 μm by DFG between the pulse trains.

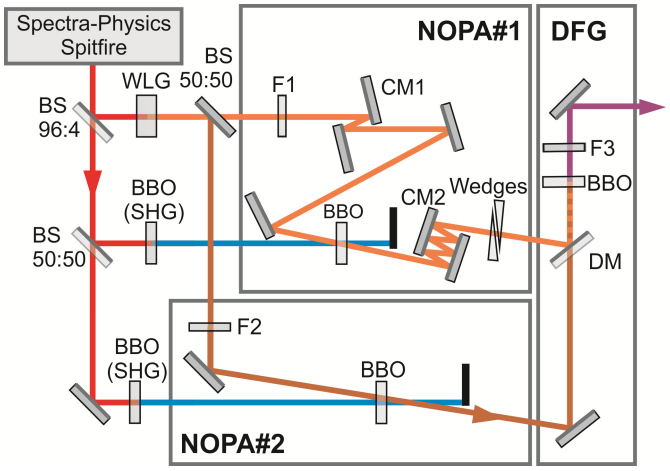

Fig. 1. Experimental setup. The system is based on pulse generation in two NOPA stages (NOPA#1, NOPA#2), which are seeded by the same white light generation (WLG) source, and subsequent difference frequency generation (DFG) of the two pulse trains. For details, see text.

A small portion of the pump light, with a pulse energy of 600 nJ, is split off and focused into a 2-mm thick sapphire plate to create a stable WL filament (white light generation, WLG in Fig. 1). The generated WL spans a spectral range from <450 nm to >1 μm and displays low power fluctuations of about 2% RMS. From the dependence of the amplification in NOPA#1 on the time delay between seed and pump, we estimate a temporal width of the WL of about 200 fs. By means of a reflective neutral density filter used as a 50:50 beam splitter (BS), the WL is split into two replicas, which serve as the seed light sources for the two NOPA stages. The major remaining fraction of the available source pulse energy serves as the pump light for the NOPAs. To this aim, the pulse train is split into two pulse trains with an energy of 220 μJ and 260 μJ, respectively, which are frequency-doubled in two 1-mm-thick β-barium borate (BBO) crystals cut for type-I phase matching. This results in two pulse trains at a center wavelength of 400 nm and with pulse energies of 110 μJ and 130 μJ, respectively.

In NOPA#1, the spectral components with wavelengths > 650 nm are suppressed by an absorptive filter (F1, 2 mm of Schott BG39), and the chirped WL is partially compressed by one reflection off a pair of chirped mirrors (CM1, Venteon DCM9) to increase the temporal overlap with the pump pulse and hence broaden the spectrum of the amplified beam. The WL and the 110-μJ second harmonic (SH) pulse train are noncollinearly overlapped in a 1-mm thick BBO crystal cut for type-I phase matching at an angle of $\theta = 32°$. In order to support a parametric gain bandwidth in excess of 100 nm, the internal angle between the SH and the

#220700 - $15.00 USD Received 8 Aug 2014; revised 26 Sep 2014; accepted 26 Sep 2014; published 9 Oct 2014

WL is set to $\approx 3.7°$ [31]. The WL is focused using a spherical mirror with 500 mm radius of curvature, and the SH light is focused by a lens of 300 mm focal length. The foci are positioned in front of the BBO crystal, such that the beam diameter of the SH and the WL inside the crystal are 650 μm and 320 μm, respectively. The peak intensity of the SH is $2.8 \cdot 10^{11}\,\mathrm{Wcm}^{-2}$. The output of NOPA#1, i.e., the amplified WL, is collimated using a second spherical mirror with 500 mm radius of curvature. The pulses are subsequently compressed by 3 reflections off a second pair of chirped mirrors (CM2, Venteon DCM9) and by transmission through a finely adjusted pair of fused silica wedges.

The seed of NOPA#2 is a fixed narrow-bandwidth pulse, which is extracted from the WL by a bandpass filter of 10 nm bandwidth, centered at 890 nm (F2, Thorlabs FB890-10). This spectral component and the 130-μJ SH pulse trains are noncollinearly overlapped with an internal angle of 2.5° in a 1-mm thick BBO crystal cut for type-I phase matching at an angle of $\theta = 29°$. The two pulse trains are focused by two lenses of 500 mm and 300 mm focal length, respectively. Again, the foci are positioned in front of the BBO crystal, such that the beam diameter of the SH and the WL inside the crystal are 650 μm and 320 μm, respectively. The peak intensity of the SH in the NOPA#2 BBO crystal is $3.3 \cdot 10^{11}\,\mathrm{Wcm}^{-2}$. The output of NOPA#2 is collimated using a 400-mm focal length lens.

The output pulse trains of NOPA#1 and NOPA#2 are collinearly combined by a dichroic mirror (DM) and are then focused with a spherical mirror with 200 mm radius of curvature into a 300-μm thick BBO crystal cut at $\theta = 30°$ for type-II phase-matched DFG. The generated DFG pulse train is collimated by a second spherical mirror with 200 mm radius of curvature, and the residual input light for the DFG stage is removed by spectral filtering (F3, Edmund Optics NT67-299).

3. Performance of the NOPA-DFG system

By changing the time delay between the WL and the SH pulse train in NOPA#1, the center wavelength of the amplified pulses can be adjusted within the wavelength range between 475 nm and 675 nm [see Fig. 2(a)]. The selected spectral band of the WL seed light is amplified to pulse energies between 0.1 μJ (for the shortest-wavelength spectrum) and 7.6 μJ (for the second spectrum from the left, centered at 525 nm). The broadest spectrum has a bandwidth of 100 nm centered at 600 nm with a pulse energy of 3.6 μJ. Pulse durations down to 7 fs are achieved.

The second NOPA#2 stage generates pulses with the center wavelength fixed to 890 nm [see black curve in Fig. 2(a)] and with a pulse energy of 2 μJ.

After suitable tuning of NOPA#1, the temporal pulse overlap between the two pulse trains in the DFG crystal is adjusted, and the conversion efficiency is optimized by slightly tilting the DFG crystal. With the fixed, narrow-bandwidth output of NOPA#2, the wide bandwidth and tunability of NOPA#1 are directly transferred to the NIR by the DFG process and result in a wavelength coverage from 1350 nm to 2030 nm [see Fig. 2(b)]. For the short-wavelength spectrum, centered at 1400 nm, a pulse energy of 220 nJ and a pulse duration of around 30 fs are achieved. For the long-wavelength spectrum, centered at 1800 nm, the pulse energy is 70 nJ and the pulse duration is 20 fs. The broadest spectrum, centered at 1600 nm, yields a pulse energy of 110 nJ and the shortest pulse duration. The duration of the NIR pulses is measured using interferometric frequency-resolved autocorrelation (IFRAC), which could also be described as a collinear FROG and which, like FROG, yields the full information on the complex electric field [32]. The IFRAC measurement yields a pulse duration as short as 10.6 fs [Fig. 3(a)], which is only slightly above the Fourier-limited pulse duration of 10.4 fs. This in agreement with the almost flat spectral phase [see Fig. 3(b)] and corresponds to 2 optical cycles.

#220700 - $15.00 USD Received 8 Aug 2014; revised 26 Sep 2014; accepted 26 Sep 2014; published 9 Oct 2014

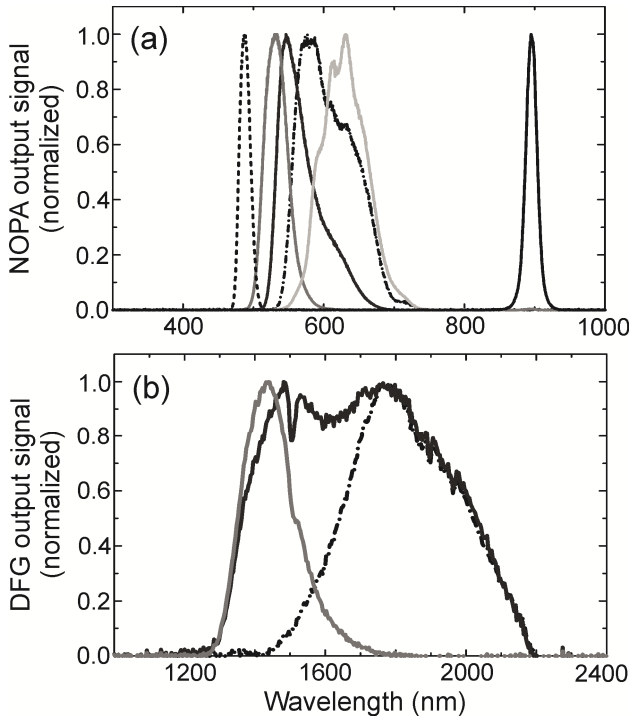

Fig. 2. Wavelength tuning of the NOPA-DFG system. (a) Output spectra of the NOPA stages. The spectra at $\lambda < 800\,\mathrm{nm}$ are generated by NOPA#1; the wavelength tuning was achieved by changing the time delay between WL and pump pulse. The spectrum at $\lambda = 890\,\mathrm{nm}$ is the output of NOPA#2. (b) DFG spectra, corresponding to the three center NOPA#1 spectra shown in (a). The detected wavelength range is limited at long wavelengths by the spectral response of the spectrometer.

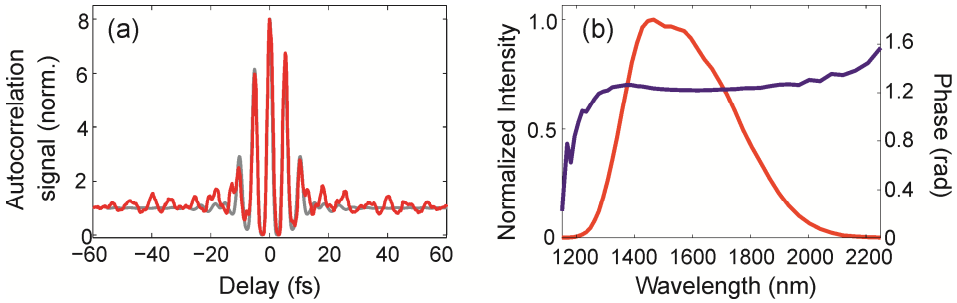

Fig. 3. (a) Interferometric autocorrelation trace distilled from an IFRAC measurement of the pulses (red curve), recorded at a center wavelength of 1.6 μm and indicating a pulse duration of 10.6 fs or 2 optical cycles. The grey curve is a simulated autocorrelation trace, calculated from the retrieved electric field strength. (b) The retrieved spectrum (red curve) indicates a Fourier-limited pulse duration of 10.4 fs, and the retrieved phase (blue curve) shows a small residual chirp.

As a measure for the beam quality, the DFG output is focused using an 0.5-NA cassegrain objective onto a sharply etched gold tip and the electron yield is measured as a function of the laser focus position on the tip. Thereby effectively the intensity distribution of the focus is measured with a near-field probe. The electron counts are displayed color-coded in Fig. 4 and show an even, almost Gaussian-shaped, and slightly elliptical distribution with a full width at half maximum of about 0.8 μm in vertical and 0.94 μm in horizontal direction. In these experiments, the electron signal scales with the fifth power of the laser intensity, $N = 5$, and

#220700 - $15.00 USD Received 8 Aug 2014; revised 26 Sep 2014; accepted 26 Sep 2014; published 9 Oct 2014

the spot size is inversely proportional to $\sqrt{N}$. The experiment thus points to a diffraction limit spot size of about 1.8 μm diameter at the fundamental.

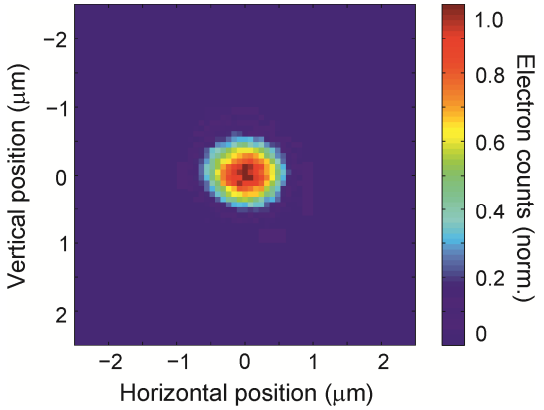

Fig. 4. Electron counts as a function of the position of the laser focus on a gold tip, with the electron count depending on the laser intensity to the fifth order. The electron counts form a slightly elliptical spot with a diameter of about 0.8 μm in vertical and 0.94 μm in horizontal direction.

4. CEP stability

Fluctuations of the CEP are measured in an f-to-2f-interferometer [33], realized as a common-path interferometer. The laser pulses are spectrally broadened to an octave-spanning bandwidth by self-phase modulation in an 8-mm thick YAG plate, followed by a 100-μm-thick BBO crystal for frequency doubling. Interference between the WL and the SH yields spectral fringes, whose period is adjusted via changing the position of the filament within the YAG crystal. A polarizer is used to project the WL and the SH to the same polarization axis and to balance their intensities. The spectral interference fringes are recorded by a monochromator equipped with a cooled CCD camera (Princeton Instruments Pro EM512B-EX), and the CEP is determined by removing high-frequency noise and by extracting the phase offset from the filtered fringe pattern.

In order to fully exploit the capability of the system to generate passively CEP-stabilized pulses, we investigated the role of different potential sources of CEP instabilities of the DFG pulses in our system. With the goal to isolate such contributions to the over-all instability, we measured time traces of different observables that could possibly act as noise sources for the CEP measurements and determined the degree of their correlation with the CEP variation by calculating the cross correlation function:

$$\phi_{sg}(\tau) = \int_{-\infty}^{\infty} s(t) \cdot g^{*}(t+\tau) dt \qquad (1)$$

Here, $s(t)$ and $g(t)$ refer to the two time traces that were compared, and τ is the delay between them. $\phi_{sg}(\tau)$ was normalized by the autocorrelation functions of $s(t)$ and $g(t)$ at time delay $\tau = 0$ to yield the normalized correlation function:

$$\varphi_{sg}(\tau) = \frac{\phi_{sg}(\tau)}{\sqrt{\phi_{ss}(0) \cdot \phi_{gg}(0)}} \qquad (2)$$

First, we ruled out that the f-to-2f interferometer itself presents a major source of instabilities, by varying the DFG pulse energy in front of the f-to-2f interferometer. Only very small changes of the spectral fringes were observed. After that, we simultaneously recorded time series of spectral fringes and time traces of either the laser SH power (at 400 nm), the

#220700 - $15.00 USD Received 8 Aug 2014; revised 26 Sep 2014; accepted 26 Sep 2014; published 9 Oct 2014

DFG power, or the duration or spectral width of the pump pulses. Varying degrees of correlations were observed. The highest degree of correlation of $\varphi(0) = 0.87$ was found between the SH power and the CEP variation. Further investigation showed that the SH and the CEP fluctuations mainly result from fluctuations in the pump pulse duration. The degree of correlation between the pump pulse duration and the CEP variation of $\varphi(0) = 0.75$ was slightly lower [see time traces in Fig. 5(a)]. Both the CEP and the SH intensity show nonlinear dependencies on the pump pulse duration: the CEP shifts with the inverse pump pulse duration, and the SH intensity is proportional to the square of the inverse pulse duration. This results in a lower degree of linear correlation $\varphi(\tau)$ between the CEP and the pump pulse duration on one hand than between the SH and the pump pulse duration on the other hand. Using a fast (~400 ms acquisition time) autocorrelator we found that the pulse duration changed slowly, on a ~2 s timescale.

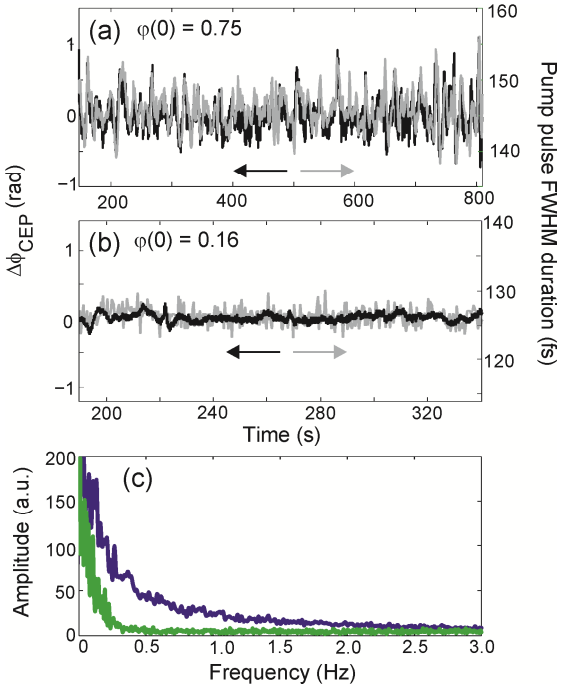

Fig. 5. (a) Initial time traces of the CEP (black curve) and of the pump pulse duration (grey curve) reveals a high grade of correlation of 0.75. (b) Measurement of the same parameters after amplifier modification show a very low grade of correlation of 0.16. (c) Fourier transforms of the CEP time traces before (blue curve) and after (green curve) amplifier modification show that slow variations in the range of 0.1 to ~3 Hz have been drastically reduced.

Heat management inside the amplifier housing emerged as a likely cause of those fluctuations. As a first attempt to improve the pulse duration stability, the amplifier was upgraded to the latest Spitfire Ace stability performance, which optimizes heat management.

After this modification of the amplifier housing we again measured the pulse duration and the CEP variation. A substantial improvement of the CEP stability was apparent: Before modification, the CEP fluctuations, when averaged over 100 ms, could be as high as ~500 mrad RMS as shown in Fig. 5(a). With the modified amplifier design, the CEP fluctuations were reduced to ~50 mrad RMS. The pump pulse duration fluctuations were reduced from 2.6 fs RMS to 1.3 fs, and the correlation between CEP noise and pump pulse duration essentially vanished [$\varphi(0) = 0.16$, Fig. 5(b)]. A Fourier transform of the CEP traces [Fig. 5(c)] shows

#220700 - $15.00 USD Received 8 Aug 2014; revised 26 Sep 2014; accepted 26 Sep 2014; published 9 Oct 2014

that mainly slow fluctuations in the range 0.1~3 Hz have been suppressed by the improved heat management.

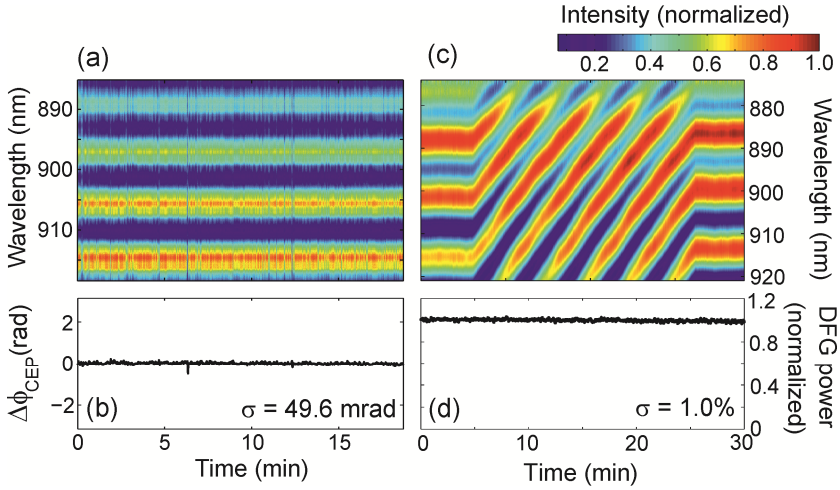

Fig. 6. (a) Interference fringes measured in the f-to-2f interferometer over a time span of 18 min when averaging over 100 pulses, showing (b) very low residual CEP fluctuations of only 49.6 mrad. (c) By inserting dispersive material, the CEP can be tuned linearly over 10π. (d) shows the power stability of the generated DFG radiation measured over 30 min, with a residual instability of about 1%.

Figure 6(a) shows spectral interference fringes recorded behind the f-to-2f interferometer over a period of 18 min. For each spectrum, the integration time was set to 100 ms (100 pulses at a repetition rate of 1 kHz). The CEP was extracted from these spectra [Fig. 6(b)], revealing low residual fluctuations of 49 mrad. This compares favorably with a previously reported measurement at a repetition rate of 100 kHz [29], and is an excellent long-term CEP stability, especially considering that it is achieved in a completely passive manner. By inserting dispersive material in the form of a pair of fused silica wedges, the CEP could be controlled and adjusted over a range of 10π [Fig. 6(c)].

So far, all characterization has been performed by temporally averaging over a series of 100 subsequent NOPA pulses and demonstrated the good long-term stability of the NOPA-DFG system. In order to be able to characterize also the short-term stability, we have also measured the CEP fluctuations from one shot to the next. For this, we recorded spectra behind the f-to-2f interferometer with the spectrometer exposure time set to 0.9772 ms, and with the laser system operating at 1 kHz repetition rate. Figure 7(a) shows a shot-to-shot measurement over 20 minutes (1200000 pulses at 1 kHz repetition rate), again displaying the good long-term CEP stability. Looking at an interval over 1 s [Fig. 7(b)] one can see, however, that there is a clear CEP fluctuation discernible between adjacent spectra. For completeness, Fig. 7(c) shows the Fourier transform of the CEP recorded over 20 minutes. One can see that the CEP noise spectrum displays a minimum at roughly 10 Hz (corresponding to averaging over 100 pulses), and is slowly increasing towards higher frequencies.

#220700 - $15.00 USD Received 8 Aug 2014; revised 26 Sep 2014; accepted 26 Sep 2014; published 9 Oct 2014

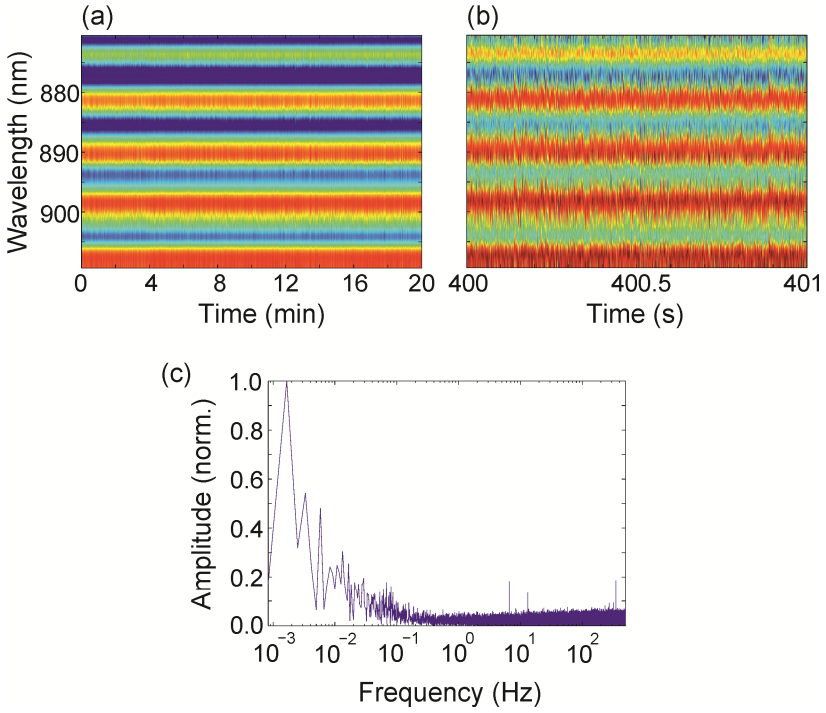

Fig. 7. Shot-to-shot CEP stability. (a) Interference fringes of single laser pulses measured in the f-to-2f interferometer over a time span of 20 minutes. (b) A zoom of a time span of 1 s makes the individual spectra visible, each recorded for a single laser pulse. (c) The Fourier transform of the CEP extracted from each spectrum shows the full CEP noise spectrum.

Thus averaging evidently suppresses high-frequency shot-to-shot fluctuations and therefore reduces the effect of CEP fluctuations on the fringes in the f-to-2f interferometer [34, 35]. To investigate high-frequency CEP fluctuations in our system, we recorded such fringes for different spectrometer exposure times. Five data sets were recorded for exposure times varying between <1 and 11 ms. In the fastest measurements, the exposure time was less than the time delay between two consecutive pulses $T = 1/f_{\mathrm{rep}} = 1\mathrm{ms}$. The results of these measurements are shown in Fig. 8, with different symbols corresponding to different exposure times and the utmost right data point of each set referring to the actual measurement. The data points further to the left result from post-processing each data set by averaging over 10, 100 and 1000 spectra, respectively, and then extracting the CEP RMS noise from the averaged spectra. For example, post-processing the shot-to-shot data by averaging over 100 spectra gives a similar result as a measurement with the integration time of the CCD camera set to capture 100 pulses. As expected from the law of large numbers, the values for the CEP noise reduce with the square root of the number of averaged pulses. Using a sensitive CCD camera as detector, we achieved count rates of around 15000 photons per pulse and could record spectral interference of single pulses. With this we can ensure that shot noise induced phase jitter of less than 10 mrad [36] is not a limiting factor in our measurements. Thus, we have measured the shot-to-shot CEP instability with an upper limit of ~800 mrad, which compares favorably with shot-to-shot CEP measurements of previously reported measurements at repetition rates at 100 Hz and 1 kHz [33, 37].

#220700 - $15.00 USD Received 8 Aug 2014; revised 26 Sep 2014; accepted 26 Sep 2014; published 9 Oct 2014

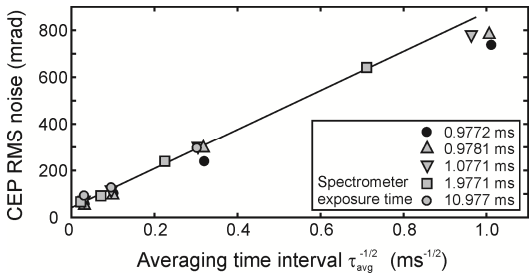

Fig. 8. Residual CEP instability extracted as a function of exposure time interval. The two utmost right data points represent shot-to-shot CEP instabilities.

We would like to note that the shot-to-shot CEP stability can also be estimated from the visibility of the fringe pattern, even when averaging over a larger number of pulses. To demonstrate this, we have simulated a large number of interference spectra with variable shot-to-shot CEP RMS noise. After averaging over 10, 100, and 1000 pulses, the average fringe visibility is plotted as the green, the red, and the blue curve in Fig. 9, respectively. In order to demonstrate the practical applicability of this method, we have extracted the fringe visibility from an experimentally measured f-to-2f interferogram, which was recorded with an exposure time of 100 ms (100 pulses). The visibility of the fringe pattern was maximized by balancing the intensity and carefully adjusting the spatial overlap of the two interfering spectral components. After careful removal of dark counts, the visibility was 0.71, which, superposed onto the red curve in Fig. 9, results in a shot-to-shot CEP RMS noise of 826 mrad. This value is in excellent agreement with the true shot-to-shot measurements presented in Figs. 7 and 8.

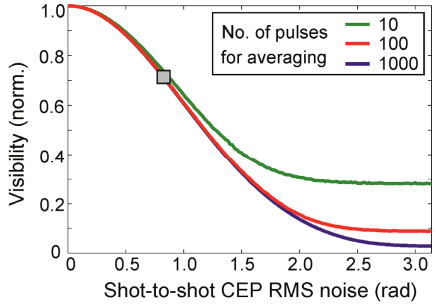

Fig. 9. Fringe visibility as a function of shot-to-shot CEP RMS noise when averaging over 10, 100, and 1000 pulses as the green, red, and blue curve, respectively. The solid curves are simulated data, and the square symbol is from a measured interference pattern, averaged over 100 pulses.

In order to demonstrate the suitability of the presented NOPA-DFG system for the observation of strong-field effects, we illuminated a sharply etched gold nanotaper with the generated NIR, CEP-controlled pulses and recorded electron kinetic energy spectra as a function of the CEP. With the pulse energy adjusted such that photoemission is governed by above-threshold ionization and the onset of strong-field emission [12, 38], the electron yield is expected to depend strongly on the maximum field strength and thus to vary with the CEP.

Figure 10 shows kinetic energy spectra of electrons that were photoemitted in this regime. The graph displays seven spectra, which were recorded, while the CEP was changed by inserting dispersive material. Between each pair of consecutively recorded spectra, the CEP was increased by $\Delta\varphi_{CEP} = \pi$. The seven recorded spectra can be clearly grouped into two sets, as indicated by the red and blue color in Fig. 10. The two sets of spectra are offset with respect to each other by a difference in CEP by $\Delta\varphi_{CEP} = \pi$. Integration of the curves yields a variation of electron counts of 50% with CEP.

#220700 - $15.00 USD Received 8 Aug 2014; revised 26 Sep 2014; accepted 26 Sep 2014; published 9 Oct 2014

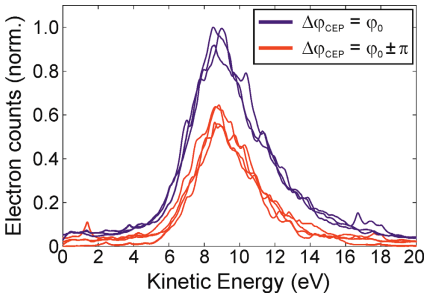

Fig. 10. Kinetic energy spectra of electrons photoemitted from a sharp gold tip. The individual curves correspond to consecutive spectra that were recorded after the CEP was increased by p. The spectra can clearly be grouped into two sets (indicated by red and blue), which are offset with respect to each other by a difference in CEP of $\Delta\varphi_{CEP} = \pi$.

At higher pulse energies, i.e., in the strong-field regime, we expect that the CEP mainly influences the field-driven acceleration of the electrons. This was confirmed by observing a cyclic variation of the cutoff energy of the kinetic energy spectra. Both observations prove that the CEP is sufficiently stable and that the pulse duration is sufficiently short to study the influence of the electric field rather than the envelope on photoemission from single nanostructures. The experiments on the CEP effect on photoemission from nanostructures in the strong-field regime can be found in [13].

5. Summary

In summary, we have realized a NOPA-DFG system as a source of few-cycle, passively CEP-stabilized NIR laser pulses. The system consists of two NOPAs, which are seeded by the same WL, followed by DFG between the outputs of the two NOPAs. The DFG output is wavelength-tunable between 1.2 and 2.1 μm and supports pulses as short as 2 cycles.

Due to the design of the system, the DFG output pulses are intrinsically CEP-stable. Furthermore, in order to reduce technical noise sources and thus to fully utilize this high potential for CEP stability, we have investigated different potential sources of CEP fluctuations. Thereby we have identified thermal fluctuations of the air within the amplifier housing as a major source, which we have suppressed successfully by improving heat management in the amplifier. This resulted in low residual CEP fluctuations of <800 mrad RMS from shot to shot, and of <50 mrad when integrating the spectra over 100 ms.

Finally, we have demonstrated the suitability of this pulsed laser source for electron photoemission from single metal nanostructures. The pulse duration was sufficiently short and the CEP sufficiently stable to clearly show a CEP dependence of electron photoemission. We believe that the development and handling of such dedicated, ultrashort pulsed laser sources is a key to observe and understand the motion of electron wave packets in solids, e. g. during electronic excitation or charge transfer processes in natural and artificial light harvesting structures.

Acknowledgments

Financial support by the Deutsche Forschungsgemeinschaft (SPP1391), by the European Union (project ‘CRONOS’, Grant number 280879-2), and the Korea Foundation for International Cooperation of Science and Technology (Global Research Laboratory project, K20815000003) is gratefully acknowledged. GC acknowledges support by the European Research Council Advanced Grant STRATUS (ERC-2011-AdG No. 291198). JV acknowledges funding from the Studienstiftung des Deutschen Volkes. JR acknowledges funding from the Deutsche Forschungsgemeinschaft (Research Training Group ‘Molecular Basis of Sensory Biology’).